Karlsruher Institut für Technologie

Inert strength measurement on silica soaked at 250°C in liquid water and water vapour

P. Hettich, S. Wagner, K. G. Schell, T. Fett

KIT SCIENTIFIC WORKING PAPERS 122

KIT – Universität des Landes Baden-Württemberg und nationales Forschungszentrum in der Helmholtz-Gemeinschaft

IAM Institute for Applied Materials

Impressum

Karlsruher Institut für Technologie (KIT)
www.kit.edu

2019

ISSN: 2194-1629

Abstract

The effect of water soaking and heat-treatment in saturated water vapour at 250°C for 192 h on the strength of silica glass is studied. Bending strength meaurements in liquid nitrogen showed a clear increase of the inert strength for heat-treated specimens over that of the untreated material. The increase in strength is interpreted as the consequence of water diffusion into exposed surfaces of the test specimen, which results in swelling of the glass and shielding of cracks, present in the surface of the glass. Experimental results are compared with theoretical predictions.

Contents

1. Introduction

In earlier publications [1-4], we explored the idea that water can toughen silica glass by diffusing into the glass structure from the crack tip. This process sets up a negative stress intensity factor that shields the crack tip and enhances the strength of the specimen. Because diffusion rates increase with temperature, crack tip shielding should also increase as the temperature is increased, as should the specimen strength. Using the model presented in [2], we explored the mechanism of crack tip shielding and showed that the calculated changes in strength resulting from water exposure at 88 °C agreed sufficiently with experimental values measured on high-silicate glass *Vycor* (Corning Inc.) by Ito and Tomozawa [5], and Hirao and Tomozawa [6]. The effects on inert strength at this rather low soaking temperature are only about 10%. In this paper, we will address the same phenomenon, but at higher temperatures of $\theta \cong 260$ °C.

Strength measurements with heat treated glass (250 °C) are in principle known from literature. Li and Tomozawa [7] soaked silica bars for up to 4 days soaking time and tested the strengths in dynamic bending tests under subcritical crack growth conditions. To the authors' knowledge, so far no really inert strength measurements are available for water-soaked silica.

1.1 Water diffusion in silica

Water diffusion into the surface of silica glass has been studied experimentally by a number of investigators, and shown to depend on temperature according to

$$D_w = A_0 \exp[-Q_w / RT] \tag{1.1}$$

where Q_w is the activation energy, T is the absolute temperature, and R is the gas constant. As reported in reference [8] for silica in the temperature range 0 °C to 200 °C: Q_w = 72.3 kJ/mol, $\log_{10} A_0$ = -8.12 (A_0 is in m^2/s).

The diffusion distance b, an appropriate measure for the thickness of the diffusion zone (where the water concentration is roughly half of that at the surface) is given by

$$b = \sqrt{D_w t} \tag{1.2}$$

(t=time).

1.2 Volume swelling

The relation between volume swelling strain ε_v and the hydroxyl concentration S (in weight units) is given by eq.(1.3)

$$\varepsilon_v = \kappa \times S \quad , \quad \kappa \cong 0.97 \tag{1.3}$$

The hydroxyl water S concentration can be computed via

$$S = \frac{17}{18}\frac{0.000780\exp\left(0.00868\,\theta\right)}{\frac{1}{2}+0.031\exp\left(\frac{10750(\mathrm{kJ/mol\,K})}{RT}\right)} \tag{1.4}$$

A volume element near the surface that undergoes swelling cannot freely expand. If the diffusion zone is small compared to the component dimensions, expansion is completely prevented in the surface plain and can only take place normal to the surface. The swelling stress at the surface, $\sigma_{sw,0}$ is then given by

$$\sigma_{sw,y} = \sigma_{sw,z} = -\frac{\varepsilon_v E}{3(1-\nu)} \tag{1.5}$$

2 Total stress intensity factor for a semi-circular surface crack

As in [4] we begin our analysis by estimating the magnitude of the total stress intensity factor, K_{tot}, experienced by the critical crack during the strength test. The total stress intensity factor consists of three contributions: K_{app}, which is primarily the result of the applied stresses and the geometry of the crack; K_{sh} which results from water penetration into all surfaces and consequently also the initial cracks of the specimen. In the absence of subcritical crack growth the condition for crack extension is $K_{tot} \geq K_{Ic}$.

In order to provide a transparent analysis we restricted the possible aspect ratios of cracks to the commonly chosen semi-circular surface crack. The depth is given by a (Fig. 1) and the aspect ratio by a/c=1. The plane of the crack is assumed to be perpendicular to the specimen length axis.

The applied stress intensity factor given by eq.(2.1) and eq.(2.2) below were derived and discussed in [9] for the case of straight specimen surfaces. Since the initial natural surface cracks are very small compared to the specimen thickness W, a/W<<1,it holds for the stress intensity factor at the deepest point (A)

$$K_{appl,A} = \sigma_{appl} 1.173\sqrt{a} \tag{2.1}$$

and for the surface points (B)

$$K_{appl,B} = \sigma_{appl} 1.29\sqrt{a}\ , \tag{2.2}$$

where in bending tests σ_{appl} is the outer fiber tensile stress. This solution can also be used for cylindrical specimens if the crack depth is small compared to the cylinder radius, a/R<<1. The crack is assumed to be at the midpoint of the test specimen, with

one axis perpendicular to the specimen length axis and the other principal axis in the plane of the specimen surface.

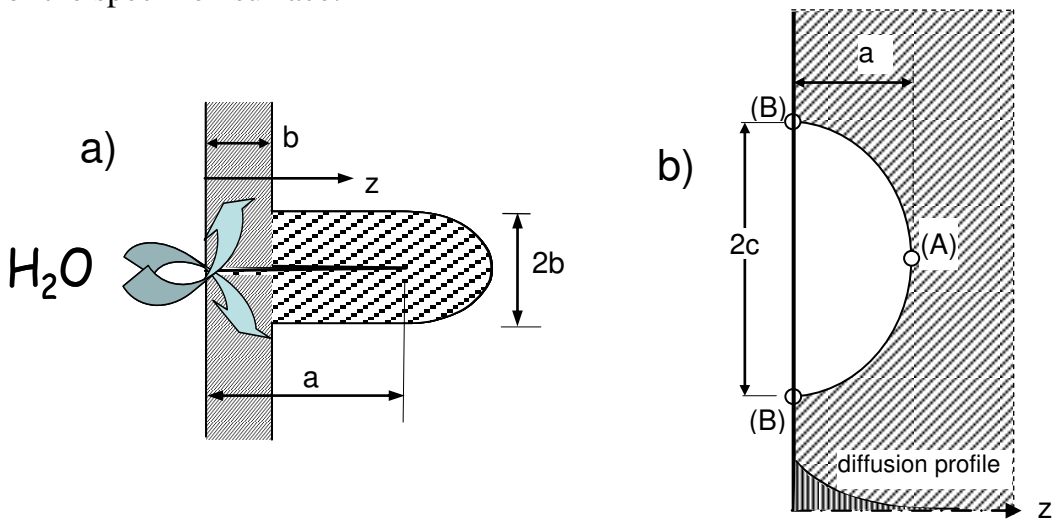

Fig. 1 Single failure relevant crack in an infinite body exhibiting a diffusion and swelling zone, a) side view, b) top view on the surface crack.

As noted above, two contributions make up the shielding stress intensity factor: one coming from the diffusion zone originating from the crack faces, the second originating from the external surfaces of the specimen.
The shielding stress intensity factors at the deepest point A and the surface points B, $K_{sh,A}$ and $K_{sh,B}$, are for $b<<R$ [4] and $0.15<b/a<1.25$

$$K_{sh,A} \cong 1.17\sqrt{a}\,\sigma_{sw,0}\tanh\left(0.698\sqrt{\frac{b}{a}}+0.317\frac{b}{a}\right) \tag{2.3}$$

$$K_{sh,B} \cong 1.29\sqrt{a}\,\sigma_{sw,0}\tanh\left(1.327\sqrt{\frac{b}{a}}+0.064\frac{b}{a}\right) \tag{2.4}$$

3. Toughness and inert strength

3.1 Apparent Toughness

The total stress intensity factors including shielding are given by

$$K_{tot,A} = K_{sh,A} + K_{appl,A} \tag{3.1}$$

$$K_{tot,B} = K_{sh,B} + K_{appl,B} \tag{3.2}$$

where $K_{appl,A}$ and $K_{appl,B}$ are obtained from eq.(2.1) and eq.(2.2); $K_{sh,A}$ and $K_{sh,B}$, from eq.(2.3) and eq.(2.4). The applied stress intensity factors for inert tests have to be computed using the initial crack dimensions a_0 and c_0.

The shielding effect is responsible for an apparent increase of the fracture toughness which is, in general, identified with the applied stress intensity factor at failure, $K_{\mathrm{appl,cr}}$. From eqs.(3.1, 3.2) the *apparent fracture toughness*, in the following denoted as $\hat{K}_{\mathrm{Ic}}$, simply results as

$$\hat{K}_{\mathrm{Ic}} = K_{appl,cr} = K_{\mathrm{Ic}} - K_{sh} \tag{3.3}$$

Since $K_{\mathrm{sh}}<0$, it holds $\hat{K}_{\mathrm{Ic}} > K_{\mathrm{Ic}}$. On the other hand it becomes clear from the fact that the inert strengths are proportional to the applied stress intensity factor, $\sigma_{\mathrm{c}} \propto K_{\mathrm{appl,cr}}$, that strength and apparent toughness increase by the same factor. In the following considerations, we therefore concentrate on the strength, exclusively. The apparent toughness for the surface and the deepest points of a semi-circular crack is shown in Fig. 2a.

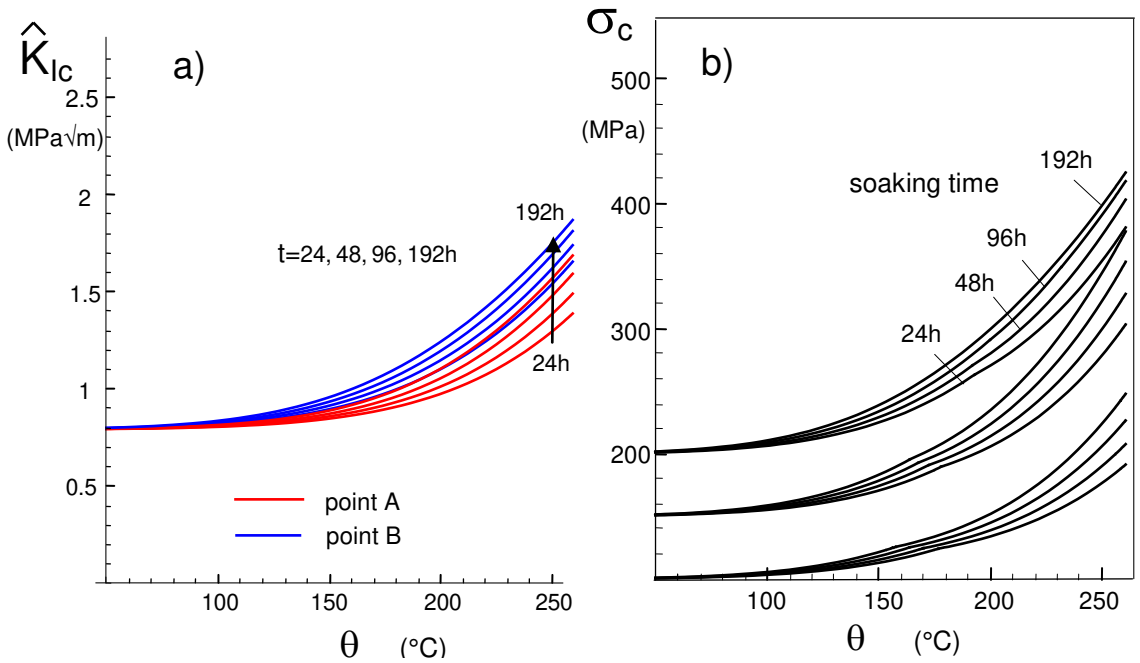

Fig. 2 a) Apparent fracture toughness after hot-water soaking for a semi-circular crack of 30 µm depth, b) calculated inert strengths as a function of water-soaking temperature θ and soaking time, predicted for inert strengths of σ_{c}=100, 150, and 200 MPa for freshly abraded test specimens.

3.2 Inert strength

Using the temperature-dependent swelling strain together with the temperature effect on the diffusivity, the inert strengths could be computed as a function of θ in the same way as outlined in [4]. The inert strength, σ_{c}, is given by the condition

$$\sigma_c = \mathrm{Min}\left(\frac{K_{\mathrm{Ic}} - K_{sh,A}}{1.17\sqrt{a}}, \frac{K_{\mathrm{Ic}} - K_{sh,B}}{1.29\sqrt{a}} \right) \tag{3.4}$$

Strength predictions are shown in Fig. 2b. For this purpose initial inert strengths were assumed to be σ_c=100, 150, and 200 MPa.

4 Strength of unsoaked and soaked specimens

We studied the strength behaviour of the silica glass EN08NB (GVB, Herzogenrath) containing 99.98% SiO_2. Cylindrical bending bars of 45 mm length were cut from silica rods of 4 mm diameter maintaining the original surface from manufacturing. Then all specimens were annealed for 1h at 1150°C in vacuum in order to eliminate pre-existing residual surface stresses. To avoid any water contact, the series foreseen for strength measurements in an inert environment were immediately, after cooling down, stored in fresh silicon oil as proposed by Sglavo and Green [10] as an inert medium. In total, two glass deliveries were considered, denoted in the following as Batch (I) and Batch (II). The soaking conditions and surface zone parameters are given in Table 1.

Batch	Time	Water	Vapour	b (µm)	S, eq.(1.4) (wt%)	ε_v	$\sigma_{sw,0}$ (MPa)
(I)	192 h	263°C	-	21.7	0.85	0.82%	-240
(II)	192 h	250°C	250°C	17.7	0.74	0.72%	-209

Table 1 Soaking conditions and properties of the water layer at the surface. $\sigma_{sw,0}$ calculated due to eqs.(1.4) and (1.5)

Inert bending strength tests were carried out in liquid nitrogen in a 3-point testing device. The results for unsoaked specimens (open circles) are shown in Fig. 3a and Fig. 3b in Weibull representation. The distributions of the unsoaked specimens show the usually expected Weibull straight–line. Applying the Maximum Likelihood procedure (for details see [11]) for Batch (I) a Weibull modulus of m = 12.3 and a characteristic strength of σ_0 = 171.3 MPa were obtained. For Batch (II) the obtained Weibull parameters are m = 6.6 MPa and σ_0 = 250 MPa. It should be noted that even if the initial strength is Weibull-distributed, the strength of specimens under swelling stresses do not necessarily result in a Weibull distribution. Because after (water or vapour) treatment, every crack has an individual apparent fracture toughness $\hat{K}_{Ic}$ (e.g. Chapter 3.1), depending on the shielding surface layer. The derivation of the Weibull-distribution however needs a constant K_{Ic} (for details see e.g. Section 10.3 in [12]). The parameters for (water/vapour) treated specimens of Batch (II), shown in Tabel 2, therefore may be denoted as *apparent Weibull parameters*.

Even the strengths of the unsoaked specimens appear rather large. The reason for this is of course the 3-point bending loading with its reduced effective surface compared to 4-point bending tests and on the other hand the circular cross section of the specimens, that reduces the effective surface once more. The strength could be described roughly

by Weibull distributions except of Batch (I) after water soaking. Table 2 shows the related Weibull parameters. Since Batch (I) shows clearly deviating behaviour, the median values as the strength parameters are compiled in Table 3. From the strengths in the untreated state and the fracture toughness of K_{Ic}=0.8 MPa√m [13], the initial crack depth a_0 can be concluded as shown in Fig. 4a and 4b.

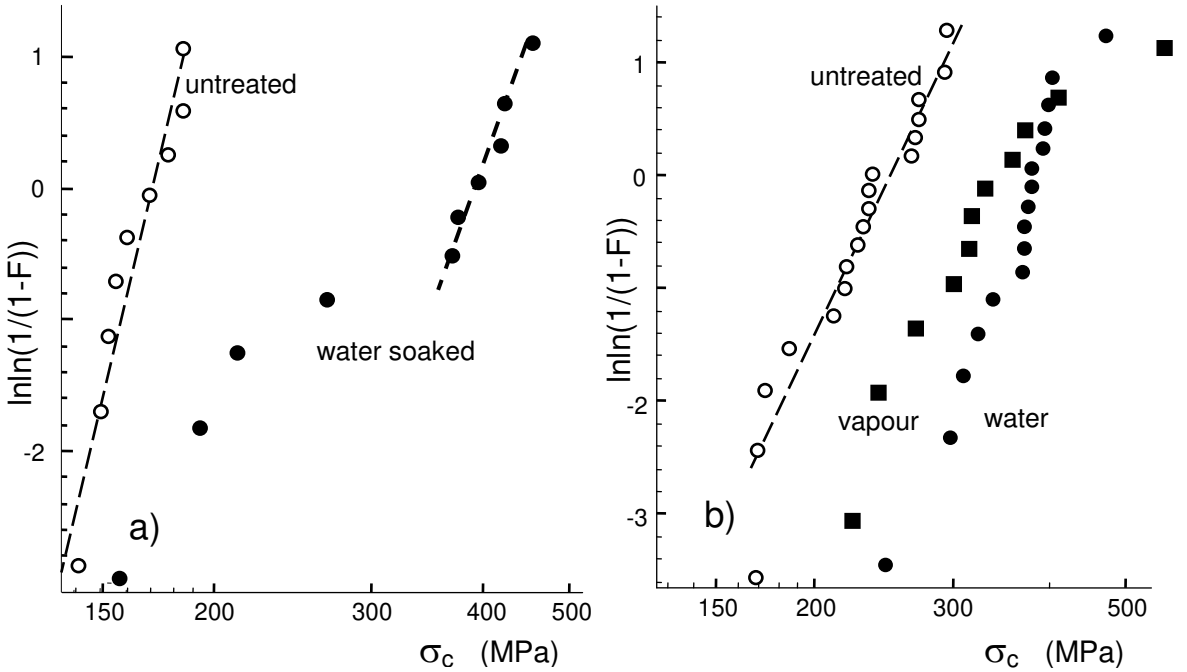

Fig. 3 3-point bending test in liquid nitrogen: Strength of untreated silica (open circles), liquid water treated (full circles), and vapour-treated specimens (squares), a) Batch (I), 263°C, b) Batch (II), 250°C.

Specimens	Batch (I)		Batch (II)	
	σ_0 (MPa)	m	σ_0 (MPa)	m
untreated	171.3	12.3	250	6.6
Water soaked	-	-	395	4.5
Vapour soaked	-	-	340	8.1

Table 2 Strength results, represented by the Weibull parameters.

Specimens	Batch (I)	Batch (II)
untreated	160.6 MPa	232 MPa
Water soaked	367 MPa	373 MPa
Vapour soaked	-	316 MPa

Table 3 Strength results, represented by the median values.

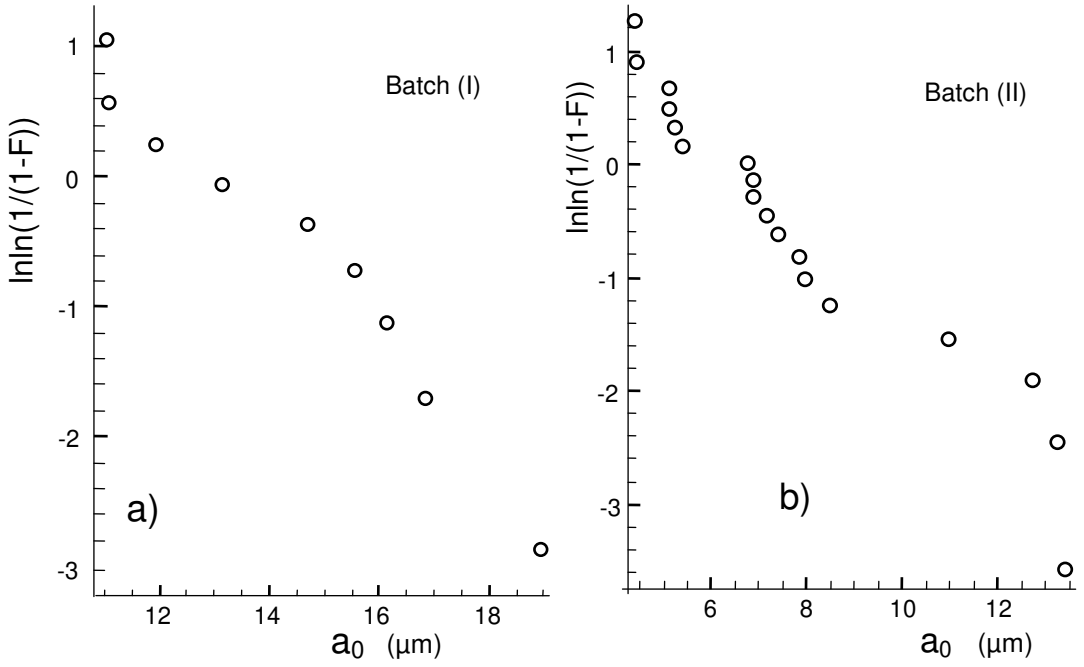

Fig. 4 Distributions of the initial crack depth a_0.

5 Strength predictions

Measurements in liquid nitrogen showed a clear increase of the inert strength for both the water-soaked and the heat-treated specimens in saturated water vapour. The results of Fig. 3 are plotted once more in Fig. 5 together with the predictions according to eqs.(2.1-3.4). The predictions were made on the basis of the Weibull distribution for the unsoaked specimens. First, the strength of the n^{th} specimen was computed for a total number of N specimens via

$$\sigma_n = \sigma_0 \left(\ln \frac{1}{1-(n-0.5)/N} \right) \tag{5.1}$$

For each selected specimen, the eqs.(2.1-3.4) were applied resulting in the predicted strength of soaked specimen corresponding to the same failure probability F. This procedure yields the red data in Fig. 5. The red arrows stand for the strength increase.

In the case of Batch (I), the lowest four strength data after soaking obviously differ clearly from the prediction showing typical features of a bimodal strength distribution. Due to their high strengths, the soaked specimens shattered in more than two fracture pieces (mostly 4-6 fragments). Therefore, it was not possible to carry out a fractographic study on the broken test pieces.

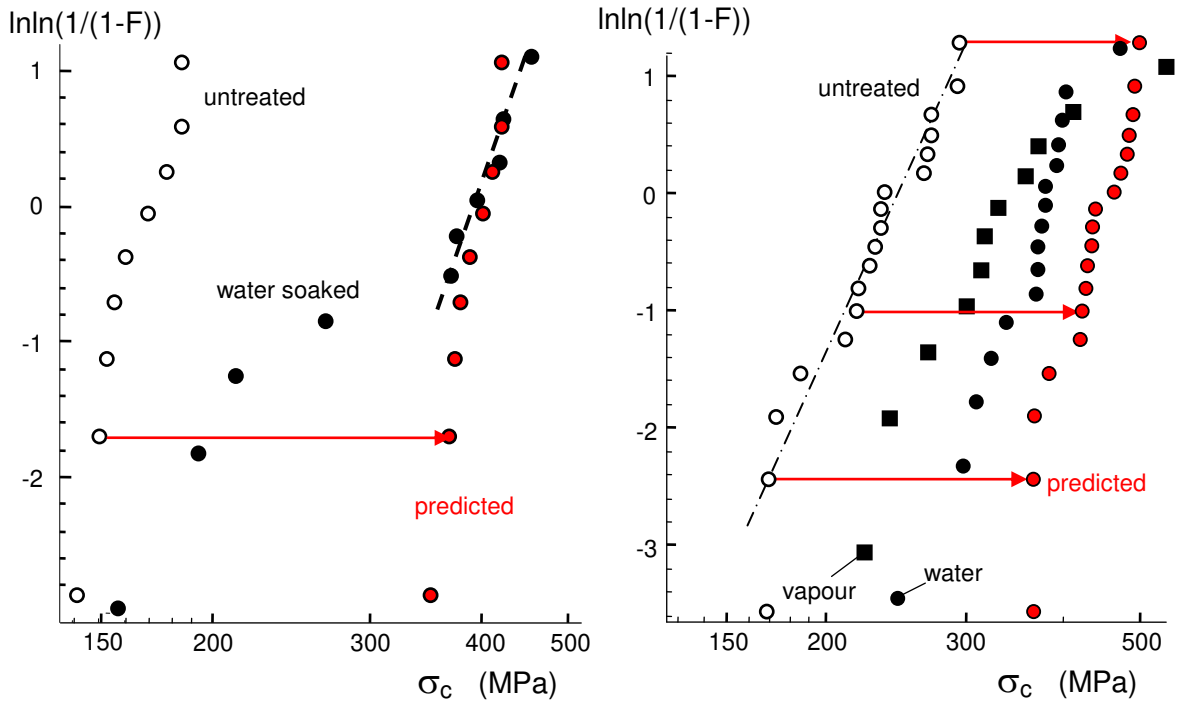

Fig. 5 Measured strengths (solid circles and squares) and predictions by the shielding stress intensity factor (red circles).

6 Analysis of nonlinear strength distributions

In the following considerations on Batch (I), it is assumed that the soaked specimens exhibit a bimodal strength distribution caused by competing of two different strength populations. Then the Weibull distributions of the strength populations "1" and "2" are given by

$$F_1 = 1 - \exp\left[-\left(\frac{\sigma_c}{\sigma_{01}}\right)^{m_1}\right] \tag{6.1}$$

and

$$F_2 = 1 - \exp\left[-\left(\frac{\sigma_c}{\sigma_{02}}\right)^{m_2}\right] \tag{6.2}$$

with the two different characteristic strengths σ_{01} and σ_{02} and the related Weibull exponents m_1 and m_2. Superposition of these strength results in the total failure probability F (for details see e.g. Section 8 in [12])

$$F = F_1 + F_2 - F_1F_2 = 1 - \exp\left[-\left(\frac{\sigma_c}{\sigma_{01}}\right)^{m_1} - \left(\frac{\sigma_c}{\sigma_{02}}\right)^{m_2}\right] \tag{6.3}$$

The Weibull parameters obtained by curve-fitting according to eq.(6.3) are compiled in Table 4. The curve fit according to eq.(6.3) is introduced in Fig. 6 by the solid curve.

The dash-dotted straight lines give the asymptotes representing the individual strength populations. The predicted strength made by using the shielding stress intensity factor is close to the measured ones of "population 1".

Strength population "1"		strength population "2"	
m_1	σ_{01} (MPa)	m_2	σ_{02} (MPa)
21.4	437.5 [404, 471]	2.7	394 [306, 482]

Table 4: Weibull parameters for the water-soaked specimens of Batch (I), 90% CI in brackets.

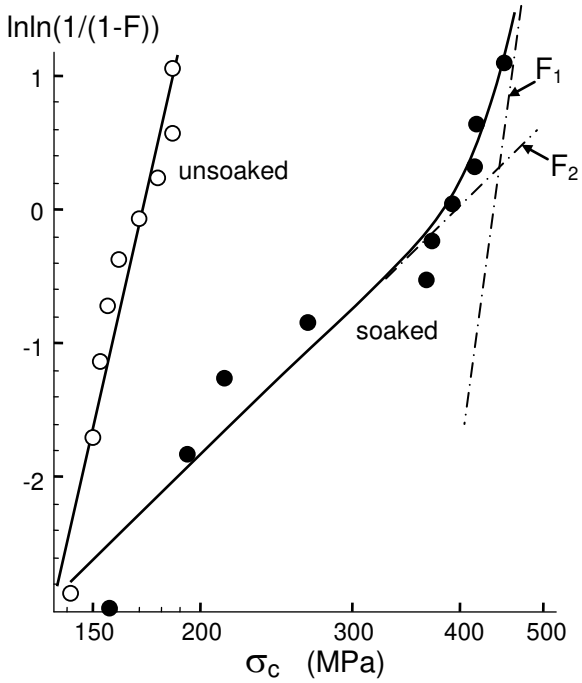

Fig. 6 Tessellation of the strengths for the hot water soaked specimens in two strength distributions (Batch (I)).

7 Reason for bimodal strength distribution

From the nearly linear shape of the strength distribution of unsoaked specimens in the Weibull plot, it can be concluded that for these results the initial failure responsible cracks were Weibull distributed, too. The bimodal strength distribution of the soaked specimens calls for an interpretation by a bimodal distribution of the failure relevant flaws. In order to discuss the observed curve shape, let us assume coexistence of surface defects (cracks) and inner flaws (pores) as schematically illustrated in Fig. 7a. The blue line indicates the strengths for the surface cracks, whereas the red line gives the strengths for the inner flaws. Under normal circumstances, the specimens will fail at the surface, because the strength is lowest there. Failure starting from internal defects

is very seldom. This is possible only when the two curves intersect at a very small failure probability F.

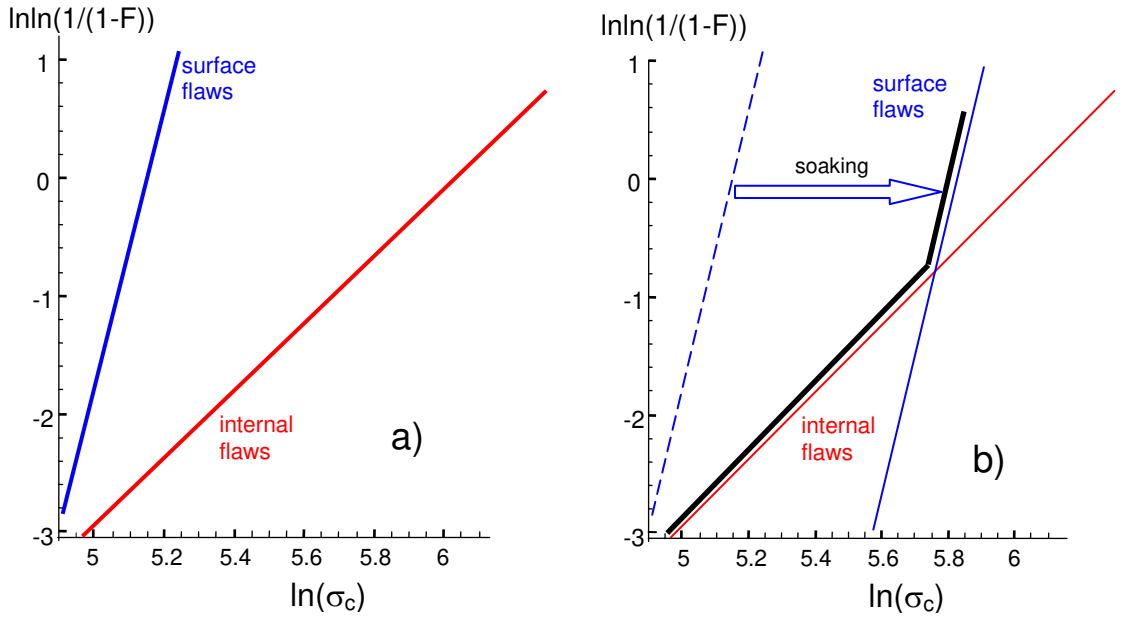

Fig. 7 a) Strength for failure starting at the surface flaws and at inner defects, b) shift of the surface strength by soaking resulting in a bimodal strength curve.

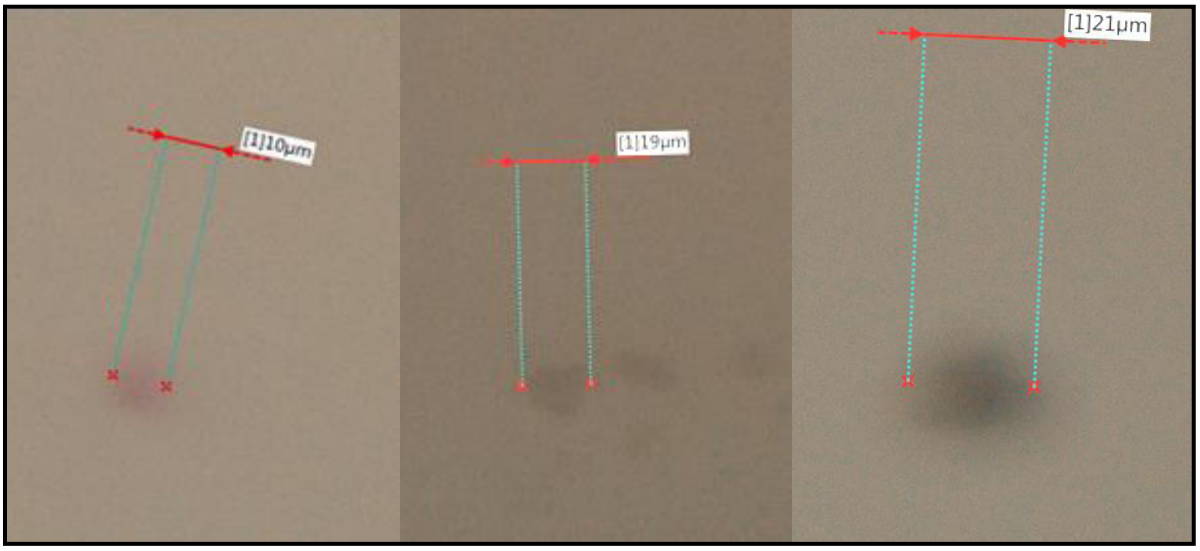

Fig. 8 Images of subsurface defects obtained with a confocal microscope.

Due to soaking, the surface is strengthened by swelling stresses. Consequently, the blue line shifts to higher strength values as indicated by the arrow in Fig. 7b. The defects below the surface zone of about 20 µm remain unaffected and can cause failure. The measurable strength is the minimum of the shifted blue and the red line. This results in the kinked black curve as found in our measurements.

Since no fractographic examination of the fracture surface was possible for the specimen fractured in liquid nitrogen, we inspected the specimens for internal flaws with a confocal microscope. Figure 8 shows subsurface defects that cannot be introduced by handling of the specimens. Their radii are about 5-10 µm. At least by this inspection technique we can confirm the existence of internal flaws competing with the surface defects on the lateral surface.

References

1 S.M. Wiederhorn, T. Fett, G. Rizzi, S. Fünfschilling, M.J. Hoffmann and J.-P. Guin, "Effect of Water Penetration on the Strength and Toughness of Silica Glass," *J. Am. Ceram. Soc.* **94** (2011) [S1], 196-203.

2 S.M. Wiederhorn, T. Fett, G. Rizzi, M.J. Hoffmann and J.-P. Guin, "The Effect of Water Penetration on Crack Growth in Silica Glass," *Engng. Fract. Mech.* **100** (2013), 3-16.

3 S.M. Wiederhorn, T. Fett, G. Rizzi, M. Hoffmann, J.-P. Guin, "Water Penetration – its Effect on the Strength and Toughness of Silica Glass," *Met. Mater. Trans. A*, **44**(2013) [3], 1164 -1174.

4 T. Fett, G. Rizzi, M. Hoffmann, S. Wagner, and S.M. Wiederhorn, "Effect of Water on the inert Strength of Silica Glass: Role of Water Penetration," *J. Am. Ceram. Soc.* **95**(2012) [12], 3847-3853.

5 S. Ito and M. Tomozawa, "Crack Blunting of High-Silica Glass," *J. Am. Ceram. Soc.* **65**(1982) [8], 368-371.

6 K. Hirao and M. Tomozawa, "Dynamic Fatigue of Treated High-Silica Glass: Explanation by Crack Tip Blunting," *J. Am. Ceram. Soc.* **70**(1987) [6], 377-82.

7 H. Li and M. Tomozawa, "Mechanical strength increase of abraded silica glass by high pressure water vapor treatment," *J. Non-Cryst. Solids* **168**(1994), 287-292.

8 Zouine, A., Dersch, O., Walter, G., Rauch, F., Diffusivity and solubility of water in silica glass in the temperature range 23-200°C, Phys. Chem. Glasses, **48** (2007), 85-91.

9 J.C. Newman and I.S. Raju, "An empirical stress intensity factor equation for the surface crack," *Engng. Fract. Mech.* **15,** 185-192, (1981).

10 V.M. Sglavo and D.J. Green, "Fatigue limit in fused silica," J. Eur. Cram. Soc. **21** (2001) 561-567.

11 Lawless, J.F. (1982): Statistical Models and Methods for Lifetime Data, Wiley, New York.

12 Munz, D., Fett, T., *CERAMICS, Failure, Material Selection, Design*, Springer-Verlag, März 1999.

13 S.M. Wiederhorn, "Fracture Surface Energy of Glass," *J. Am. Ceram. Soc*., **52**[2], 99-105, (1969).

KIT Scientific Working Papers
ISSN 2194-1629

www.kit.edu